JOURNAL OF APPLIED ELECTROCHEMISTRY 17 (1987) 294–302

*Electroplating silicon and titanium in molten fluoride media**

J. DE LEPINAY, J. BOUTEILLON, S. TRAORE, D. RENAUD, M. J. BARBIER

Centre de Recherche en Electrochimie Minérale et Génie des Procédés, U.A. au CNRS 1212, B.P. 75, Domaine Universitaire, 38402 St Martin d'Heres Cedex, France

Received 10 April 1986; revised 1 July 1986

The electrolytic reduction mechanisms of K_2SiF_6 and K_2TiF_6 solutions in LiF–KF and LiF–NaF–KF eutectic mixtures have been studied at temperatures between 550 and 850° C.

The reduction of K_2SiF_6 proceeds by two successive electron transfers,

$$Si(IV) + 2e \longrightarrow Si(II) + 2e \longrightarrow Si$$

coupled with an antidisproportionation reaction

$$Si(IV) + Si \underset{k_b}{\overset{k_b}{\rightleftharpoons}} 2Si(II)$$

Very pure thin silicon layers, up to 300 μm thick, were obtained on a silver substrate.

The cathodic reduction of TiF_6^{2-} ions occurs in two well separated reversible steps,

$$TiF_6^{2-} + e \longrightarrow TiF_6^{3-} + 3e \longrightarrow Ti + 6F^-$$

Adherent coatings of pure titanium were found to be linked to the copper substrate by an interdiffusion sublayer comprising Ti_2Cu, TiCu, Ti_2Cu_3 and $TiCu_4$ which were formed in a narrow potential domain preceding titanium deposition.

1. Introduction

The complexing power of molten fluorides is particularly favourable to the electrowinning of reducing elements such as silicon and the refractory metals which form highly volatile chlorides. Furthermore, these media lead to more dense and coherent electrodeposits than other molten salt mixtures [1, 2].

Recently, several authors [3–13] have focused attention on the electrolysis of alkali metal fluorosilicates as a new route to the production of cheap pure silicon suitable for photovoltaic uses. From the recent survey by Monnier [14] it appears that the reduction mechanism is still under discussion.

Much work has been performed on the electrolytic production of pure titanium in molten halides. However, little information exists regarding the electrode process in fluoride melts [15] and titanium electroplating techniques [16–21]. The growth mechanism of titanium layers on other metals has not been studied.

In this paper we present the results of voltammetric studies on the electrolytic reduction mechanisms of K_2SiF_6 and K_2TiF_6 solutions in LiF–KF and LiF–NaF–KF eutectic mixtures. Some pictures of pure silicon and pure titanium electroplates are also shown.

The general purpose experimental set-up has been described previously [12, 22].

2. Electrolytic fluorosilicate reduction

2.1. *The reduction mechanism*

Silver was chosen as the electrode material since it is completely insoluble in silicon [23]. Poten-

* This paper was presented at a workshop on the electrodeposition of refractory metals, held at Imperial College, London, in July 1985.

0021-891X/87 $03.00 + .12

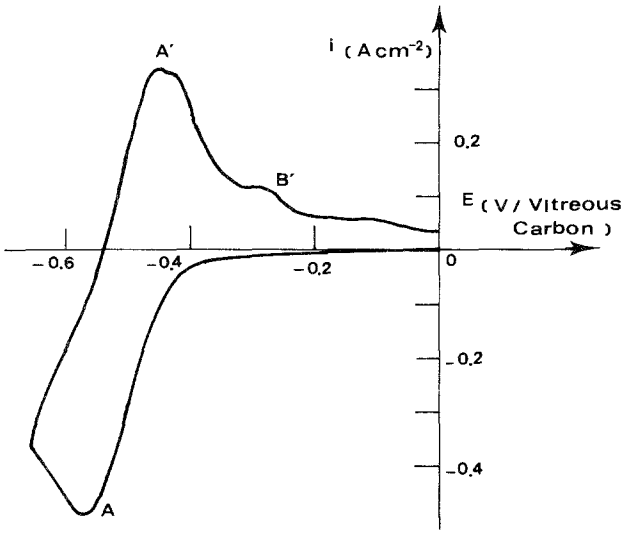

Fig. 1. Voltammetric reduction of SiF_6^{2-} in molten Flinak at 750° C. $X_{K_2SiF_6} = 2 \times 10^{-3}$; $V = 0.1\,V\,s^{-1}$; $0\,V \rightarrow -0.65\,V \rightarrow 0\,V$ versus vitreous carbon.

tials are referred to the silicon quasi-reversible electrode potential except when another is specified.

Fig. 1 presents a voltammogram obtained with a 2×10^{-3} M solution. The reduction peak A is visible along with a peak A′ and a wave B′ during oxidation; the anodic current is significant over a wide anodic potential range. Two species are likely to be involved during reoxidation.

In Fig. 2 we present a current reversal chronopotentiogram showing two transitions. For curves a and b, the current was inverted before the first transition. The ratio between the backward time and the forward time is approximately one-third. This means that oxidized and reduced species are both soluble. When the current is inverted after the first transition time (curve c) the ratio increases but remains less than unity. This second transition seems to be related to the formation of an insoluble species with kinetic complications. We suppose that the insoluble product is partly consumed by a coupled chemical reaction.

Fig. 3 shows voltammograms, obtained with a 2×10^{-3} M solution, for increasingly cathodic scan limits. Regarding Fig. 3a, we verified that the peak C′ was present before fluorosilicate addition to the melt. The wave B′ corresponds to the oxidation of a soluble species which does not

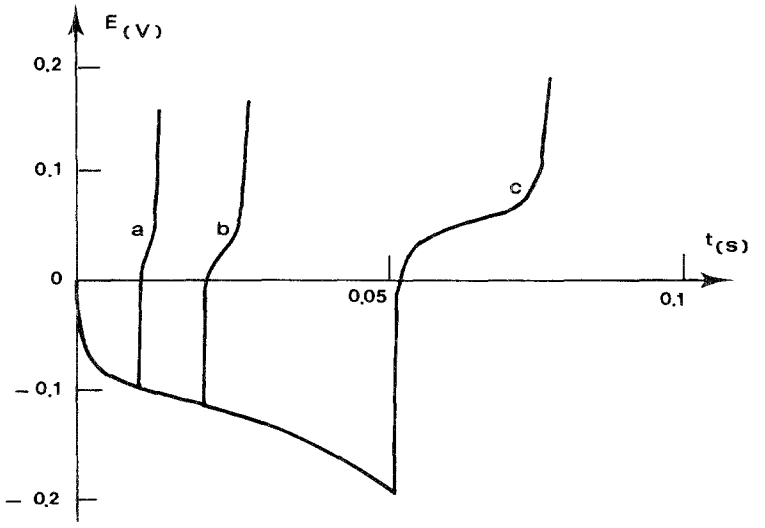

Fig. 2. Current reversal chronopotentiogram for K_2SiF_6 reduction in molten Flinak at 750° C. $X_{K_2SiF_6} = 5 \times 10^{-4}$; $i_a = -i_c = 200\,mA\,cm^{-2}$.

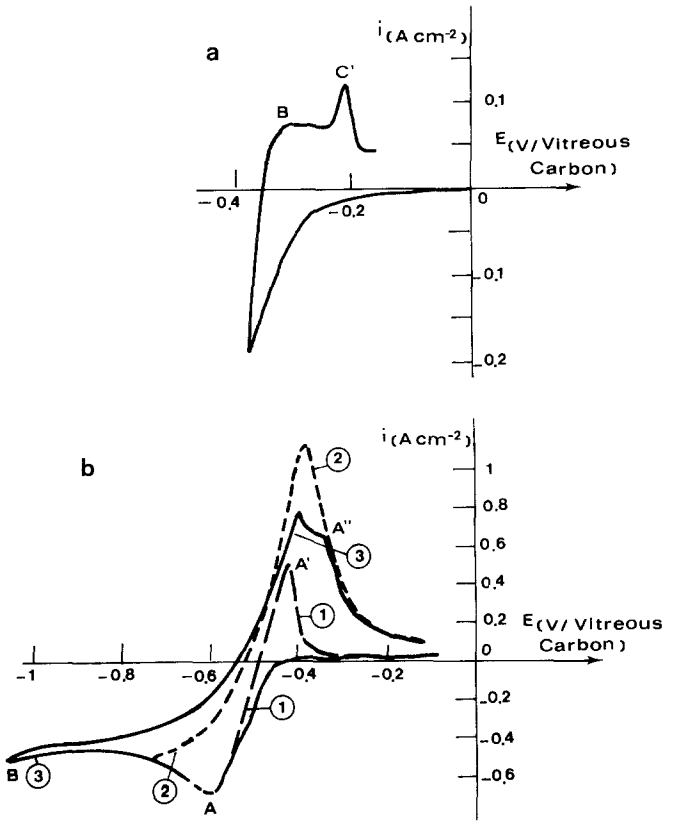

Fig. 3. Voltammetric reduction of SiF_6^{2-} in molten Flinak at 750° C. $X_{K_2SiF_6} = 2 \times 10^{-3}$; $V = 0.1\,V\,s^{-1}$. (a) Scan after a potential step at -0.4 V versus vitreous carbon, during 10 s; 0 V → -0.4 V → 0 V versus vitreous carbon. (b) 0 V → E_λ → 0 V versus vitreous carbon with (1) $E_\lambda = -0.5$ V; (2) $E_\lambda = -0.7$ V; (3) $E_\lambda = -1.5$ V.

accumulate on the electrode surface during a potentiostatic step. With regard to Fig. 3b, the anodic stripping peak A′ first rises as the cathodic limit is made increasingly negative, then decreases when the limit becomes more cathodic than -0.7 V versus the vitreous carbon electrode potential. When the potential is stepped in the first domain, the product accumulates and a pure silicon deposit forms on the electrode surface. In the other domain, alkali metal is formed and dissolves in the fluoride melt where it alloys with silicon to give soluble silicides. To summarize, the process involves two steps and an intermediate soluble species is formed.

The presence of Si(II) species in the melt has been suggested [5, 14]. These species result from the partial reduction of the fluorosilicate by pure silicon. To investigate the mechanism we studied the influence of the sweep rate and compared the resulting curves to the simulated theoretical curves corresponding to the possible mechanisms.

Fig. 4 represents the variation of the $iv^{1/2}$ product versus the potential deduced from voltammograms for a 2×10^{-4} M solution. Depending on the sweep rate, two families of curves can be distinguished. Within each family the $iv^{-1/2}$ curves are virtually identical, demonstrating that each system behaves reversibly.

Using Feldberg's finite difference method [24] with some modifications [13], we computed the theoretical curves corresponding to the follow-

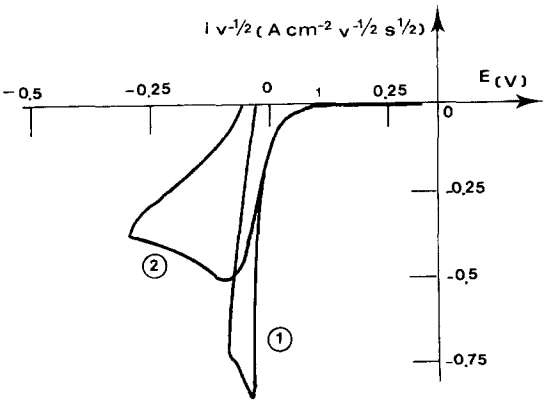

Fig. 4. Voltammetric curves typical of the two reduction mechanisms. $X_{K_2SiF_6} = 2 \times 10^{-3}$. (1) Scan rate: $60\,V\,s^{-1}$ + 0.3 V → -0.3 V → -0.05 V. (2) Scan rate: $0.1\,V\,s^{-1}$ + 0.3 V → -0.1 V → -0.025 V.

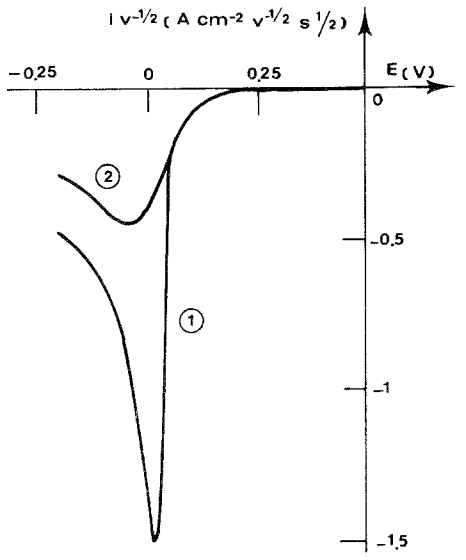

Fig. 5. Theoretical voltammetric curves of the proposed EEC_s mechanisms. $\Delta E^0 = 50$ V; temperature: 750° C.

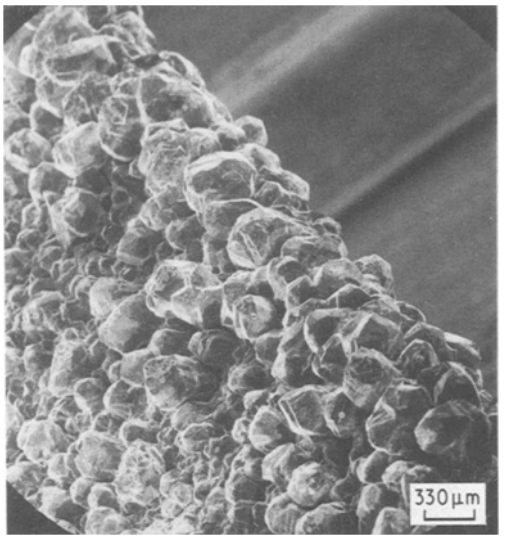

Fig. 6. Scanning electron micrograph of a silicon deposit. $X_{K_2SiF_6} = 0.05$; $-i_c = 20\,mA\,cm^{-2}$; $t_c = t_r = 2$ s, $t_a = 0$.

ing EEC_s mechanism:

$$Si(IV) + 2e \rightleftharpoons Si(II) \quad \text{(reversible)}$$

$$Si(II) + 2e \rightleftharpoons Si \quad \text{(quasi-reversible)}$$

$$Si(IV) + Si \underset{k_b}{\overset{k_f}{\rightleftharpoons}} 2Si(II)$$

The comparison of the experimental and theoretical curves (Fig. 5) supports the proposed mechanism. Other mechanisms were assumed but gave results which cannot account for our experimental results.

2.2. *Silicon electroplates*

We first present some general observations concerning silicon electrodeposition.

(i) To avoid alkali metal silicide formation, the potential step should be as little negative as possible.

(ii) Electrolytic silicon is not obtained unless the solvent is first purified.

(iii) A pulsed current gives the best fit between electrolysis conditions and the mechanism. It is known that a pulsed current is beneficial to the structure of the deposit [25]. The Si(II) species concentration near the electrode surface can be kept constant using a current profile with a cathodic pulse followed by a rest time. A short anodic pulse can be included to increase the purity of the deposit since some of the impurities contained in the deposit are periodically dissolved.

The deposits are smooth (Fig. 6). The silicon layer growth reaches several µm per hour and the thickness of the layers amounts to 0.3 cm.

Fig. 7 shows a cross-section perpendicular to the electrode surface. The silicon chemical purity was analysed by neutron activation [26]. The

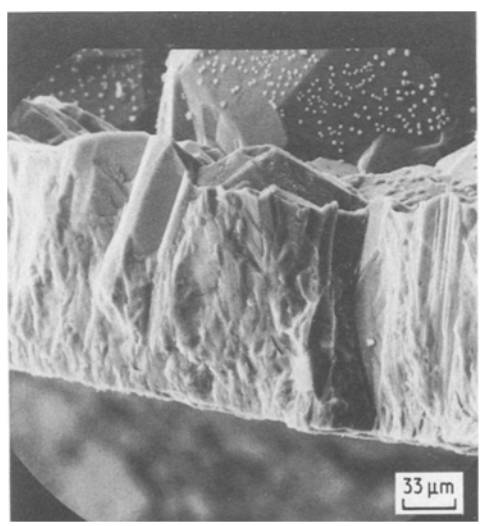

Fig. 7. Scanning electron micrograph of a silicon deposit cross-section. $X_{K_2SiF_6} = 0.1$; $-i_c = i_a = 40\,mA\,cm^{-2}$; $t_c = 60$ s, $t_r = 30$ s, $t_a = 1$ s.

amounts of typical impurities (iron, chromium, molybdenum, alkali metals [12]) are less than p.p.m.

3. Electrolytic fluorotitanate reduction

3.1. *The reduction mechanism*

The TiF_6^{2-} ions are reduced to titanium metal by two well-separated electrochemical steps [15, 22]; the first gives TiF_6^{3-} ions [22] whereas the second produces titanium metal [27] at potentials $+0.4$ V more positive than the final reduction of potassium fluoride into pure metallic potassium. The potentials reported in this section are all referred to the potassium ion–pure potassium metal equilibrium in the melt.

As a result of the high current densities flowing through the electrodes, the voltammetric transients are altered by the ohmic drop interference and were consequently processed using convolution techniques [28, 29]. The reversibility and the main characteristics of the TiF_6^{2-}–TiF_6^{3-} equilibrium were measured [20, 25] in this way.

The trivalent titanium solutions were prepared by connecting the nickel crucible to a titanium rod partly immersed in the bath during the addition of K_2TiF_6 pellets. The TiF_6^{2-} ions are completely reduced to the trivalent state according to:

$$3TiF_6^{2-} + Ti + 6F^- \longrightarrow 4TiF_6^{3-}$$

The reduction process was followed by recording successive voltammetric curves or the corresponding semi-integral curves in the domain of the tetravalent–trivalent titanium equilibrium [25].

The reduction mechanism of TiF_6^{3-} ions was studied on molybdenum and copper electrodes. Molybdenum was selected on the grounds of the low values expected for interdiffusion coefficients between refractory metals, whereas copper was chosen for its possible use in the dimensionally stable anodes (DSA) field.

Fig. 8 permits a direct comparison between the electrochemical behaviours of molybdenum (curve a) and copper electrodes (curve b). The reduction peak C on molybdenum presents a shape corresponding to the formation of insoluble species which is confirmed by a sharp stripping peak C′ during the anodic reverse scan. On the other hand, on copper electrodes, reduction begins at potentials about 80 mV more positive than on molybdenum, and several humps precede the main reduction peak which occurs at the same potential as on molybdenum. During the reverse scan, after the first stripping peak corresponding to the oxidation of pure titanium, the other peaks are assigned to the anodic dissolution of different intermetallic copper–titanium compounds.

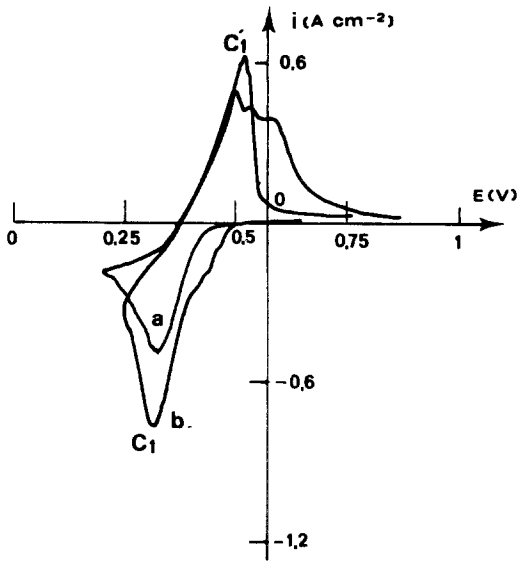

Fig. 8. Voltammetric reduction of TiF_6^{3-} solutions in molten Flinak at 600° C. $X_{TiF_6^{3-}} = 2 \times 10^{-2}$; $v = 10^{-2}$ V s^{-1}. (a) Molybdenum; $+0.65$ V → $+0.20$ V → $+0.80$ V. (b) Copper; $+0.65$ V → $+0.25$ V → $+0.85$ V.

The reduction mechanism of the TiF_6^{3-} species was characterized for molybdenum, on which it seems to proceed through a single step without alloy formation. The reversibility test (Fig. 9) was performed by comparison of the semi-integral curves of voltammograms recorded at different sweep rates. All the curves are very close; moreover, they are almost the same during the direct and the reverse scan in the cathodic overpotentials domain. This behaviour confirms that the electron exchange is very fast.

According to the Nernst relation between the concentration of solute species and the electrode potential, it follows that:

$$E = E_{th} + \frac{RT}{nF} \ln \frac{m^* - m}{m^*}$$

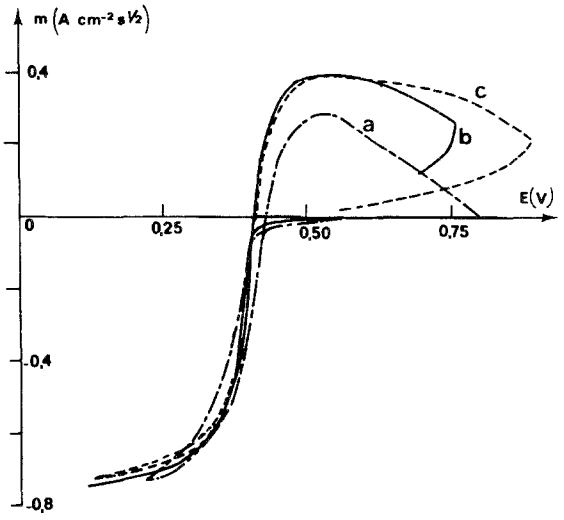

Fig. 9. Semi-integral transforms of reduction voltammograms obtained at different sweep rates. Flinak + TiF_6^{3-} ($X = 5 \times 10^{-2}$); $T = 700°C$. Molybdenum electrode. (a) $v = 0.2\,V\,s^{-1}$; (b) $v = 0.5\,V\,s^{-1}$; (c) $v = 1\,V\,s^{-1}$.

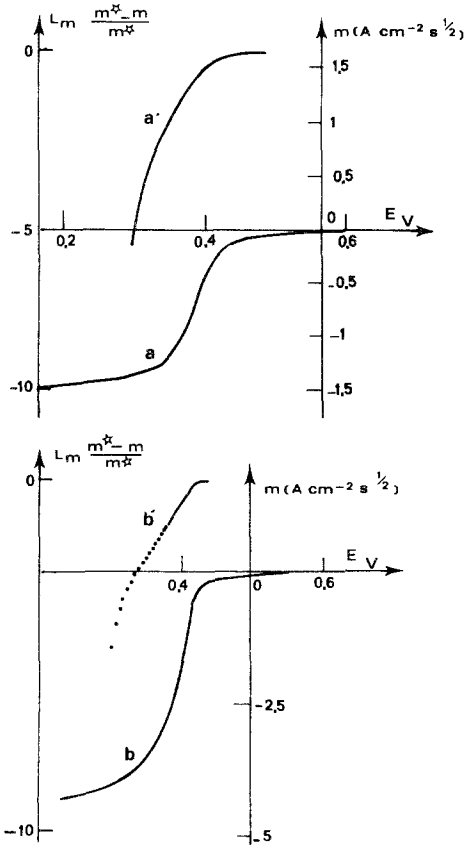

Fig. 10. Semi-integration convolution analysis of reduction voltammograms obtained at $0.1\,V\,s^{-1}$. Flinak + TiF_6^{3-} (X); Molybdenum electrode. (a, a′) $T = 600°C$; $X = 2 \times 10^{-2}$; (b, b′) $T = 700°C$; $X = 5 \times 10^{-2}$. (a) and (b) are semi-integrated voltammograms; (a′) and (b′) are the logarithmic analysis of the corresponding semi-integrated voltammograms.

where E_{th} is the equilibrium potential of titanium metal with the TiF_6^{3-} solution, m is the semi-integral of the current density [28, 29] and m^* is the cathodic limiting value of this function obtained at high cathodic overpotentials. This has been verified at $T = 600°C$ (Fig. 10a, a′) and at $T = 700°C$ (Fig. 10b, b′). Fig. 10 presents the semi-integral curves (a, b) and the corresponding logarithmic transforms (a′, b′). The slope of the linear part of the curves a′ and b′ yields the number of electrons exchanged during the TiF_6^{3-}

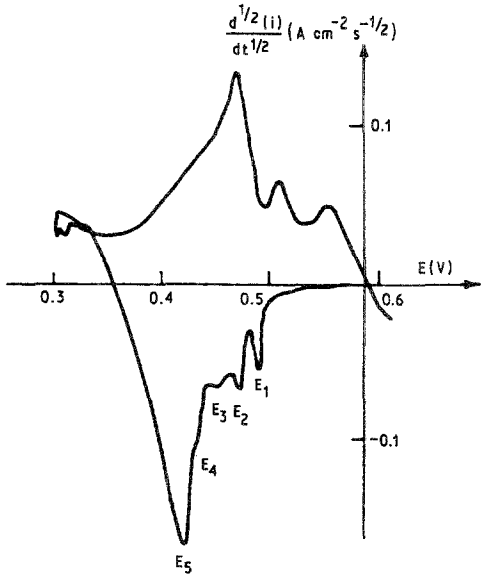

Fig. 11. Semi-derivative transform of the voltammogram presented in Fig. 8b.

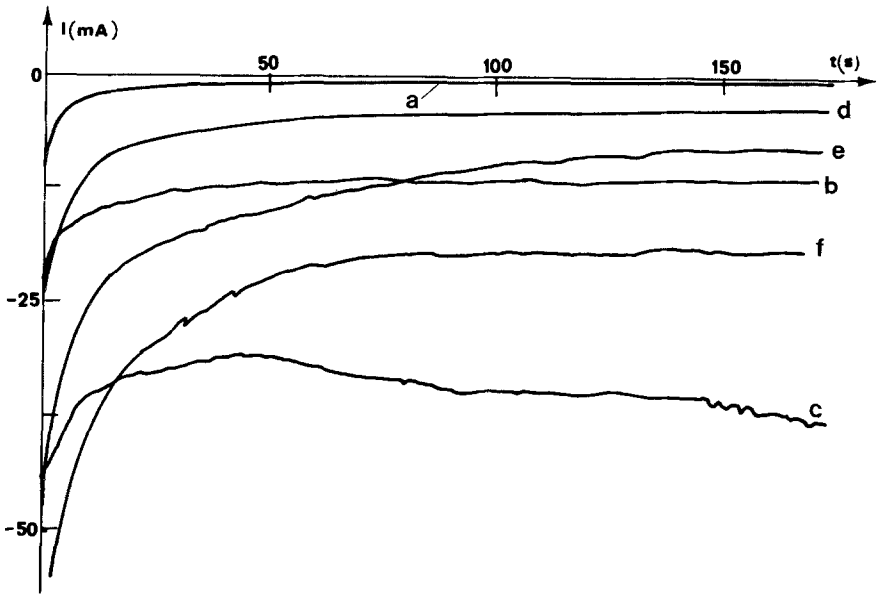

Fig. 12. Current–time transients during cathodic potentiostatic polarizations of molybdenum and copper electrodes. Flinak + TiF_6^{3-} ($X = 5 \times 10^{-2}$); $T = 700°C$. (a) Mo; $E = +0.49$ V; (b) Mo; $E = +0.45$ V; (c) Mo; $E = +0.41$ V; (d) Cu; $E = +0.53$ V; (e) Cu; $E = +0.49$ V; (f) Cu; $E = +0.45$ V.

reduction, i.e. $n = 2.9 \pm 0.3$. Therefore, the cathodic reduction of TiF_6^{3-} ions to titanium metal proceeds reversibly through the direct exchange of three electrons without any intermediate step.

On copper electrodes, alloy formation precedes the deposition of pure titanium. The semi-derivative analysis (Fig. 11) of the voltammetric curve shown in Fig. 8b gives a good estimation of the apparition potentials of new phases which are supposed to be intermetallic compounds. In Fig. 11, obtained at 700° C with a 2×10^{-2} M TiF_6^{3-} solution, we observe four peaks: E_1 at $+0.495$ V, E_2 at $+0.48$ V, E_3 at $+0.45$ V, and E_4 at $+0.43$ V preceding the pure titanium formation peak E_5 at $+0.42$ V.

The metalliding process involving the incorporation of titanium atoms into the copper lattice is clearly shown in Fig. 12 by a comparison of the potentiostatic transients recorded using a copper electrode (curves d to f) and a molybdenum electrode (curves a to c). The current observed with the copper electrode is much higher than with molybdenum when the poten-

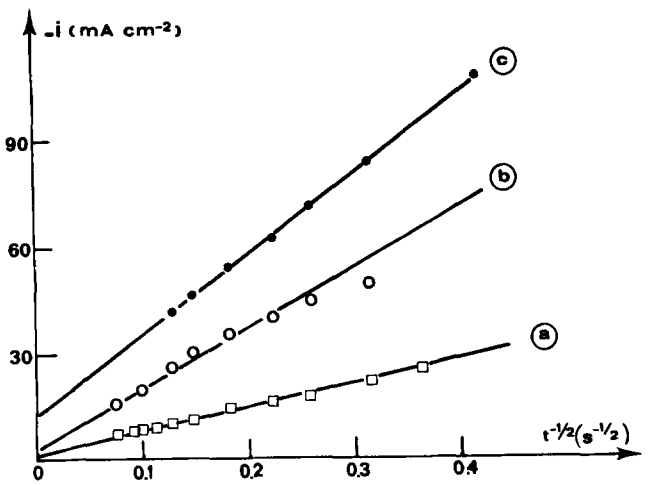

Fig. 13. Analysis ($I = f(t^{-1/2})$ of the potentiostatic transients during the reduction of TiF_6^{3-} onto copper electrodes at more positive potential than the TiF_6^{3-}–titanium equilibrium potential. Flinak + TiF_6^{3-} ($X = 5 \times 10^{-2}$); $T = 700°C$. (a) $E = +0.53$ V/K^+–$K = +0.08$ V/TiF_6^{3-}–Ti; (b) $E = +0.49$ V/K^+–$K = +0.04$ V/TiF_6^{3-}–Ti; (c) $E = +0.45$ V/K^+–$K = +0.00$ V/TiF_6^{3-}–Ti.

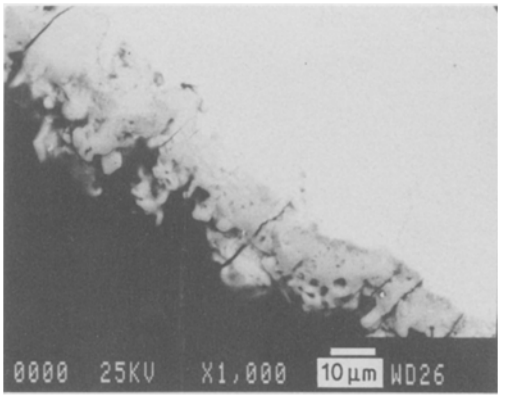

Fig. 14. Cross-section of an oxygen-contaminated titanium coating on copper. Flinak + TiF_6^{3-} ($X = 5 \times 10^{-2}$); $T = 600°C$; $I = 39\,mA\,cm^{-2}$.

tial is maintained more positive than the TiF_6^{3-} – titanium metal equilibrium (i.e. $+0.45\,V/K^+ - K$). Moreover, the current at the copper electrode decreases steadily over more than 10 min; this is typical of kinetics by the diffusion of atoms inside the metallic phase. In this potential range we obtain (Fig. 13) a linear relationship between the current and $t^{-1/2}$, showing that Cottrell's law is obeyed. On the other hand, the current is rapidly controlled by convection in the salt as soon as the potential is slightly cathodic with respect to the TiF_6^{3-}–Ti equilibrium (Fig. 12f), as is the case for molybdenum (Fig. 12b, c).

3.2. *Titanium electroplates*

Owing to the good fluxing qualities of molten fluorides, the metallic substrate can initially be very clean. However, the oxygenated species formed in the melt must be totally removed; if not, the first layers of the deposit are always titanium oxides or sheets of titanium with a good deal of oxygen inserted along the c axis of the hexagonal lattice. When the bath is less contaminated we obtain porous layers of pure titanium with many cracks (Fig. 14).

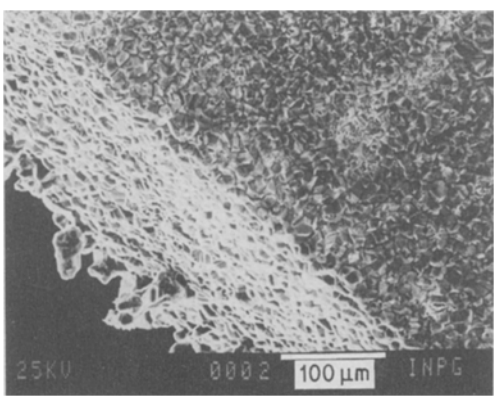

Fig. 15. Titanium deposit obtained on a copper electrode in a pre-electrolysed solution.

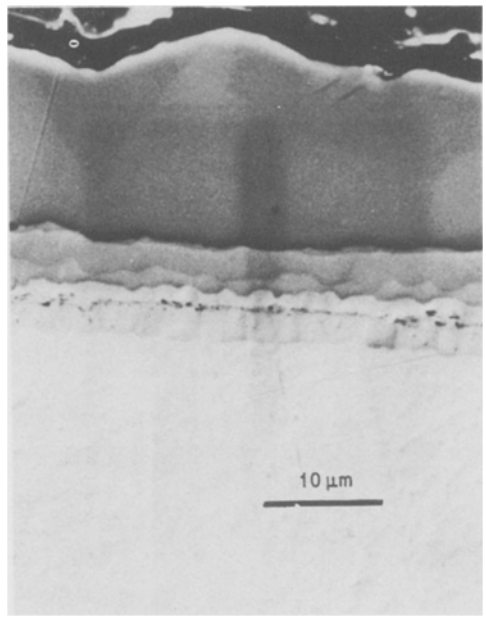

Fig. 16. Cross-section of a titanium coating on copper. Flinak + TiF_6^{3-} ($X = 9.5 \times 10^{-3}$); $T = 765°C$; $I = 150\,mA\,cm^{-2}$.

Pre-electrolysis of the solution, with a copper cathode and a titanium anode can be used to eliminate the oxygenated impurities. In this way the electrode can be completely plated (Fig. 15) with a very dense deposit presenting well-crystallized grains of an average size of 20–50 μm. This thickness of pure titanium layers obtained amounted to $30\,\mu m\,h^{-1}$ and adherence was ensured by the formation of a multilayer diffusion zone joining the pure titanium to the copper substrate (Fig. 16). The thickness of the intermetallic diffusion underlayer increased from 5 to 15 μm per hour as the temperature was raised from 700 to 800° C. Its structure was determined by X-ray microanalysis in the electron microscope and by an electron microprobe. Starting from the copper bulk electrode, the layers are successively: copper–titanium solid solution, Cu_4Ti, Cu_3Ti_2, TiCu and Ti_2Cu.

References

[1] G. W. Mellors and S. Senderoff, *J. Electrochem. Soc.* **112** (1965) 266.
[2] D. Inman and S. H. White, 'Molten Salts Electrolysis in Metal Production', Int. Symp. Grenoble, Inst. Min. Metall. London (1977) p. 51.
[3] U. Cohen and R. A. Huggins, *J. Electrochem. Soc.* **123** (1976) 381.
[4] U. Cohen, *J. Electronic Mater.* **6** (1977) 607; US Patent 3983012 (1976).
[5] R. Boen, Thèse, Grenoble (1979).
[6] G. M. Rao, D. Elwell and R. S. Feigelson, *J. Electrochem. Soc.* **127** (1980) 1940.
[7] *Idem, ibid.* **128** (1981) 1708.
[8] *Idem, ibid.* **130** (1983) 1021.
[9] R. C. Mattei, D. Elwell and R. S. Feigelson, *ibid.* **128** (1981) 1712.
[10] D. Elwell and G. M. Rao, *Electrochim. Acta* **27** (1982) 676.
[11] K. L. Carleton, J. M. Olson and A. Kibber, *J. Electrochem. Soc.* **130** (1983) 782.
[12] R. Boen and J. Bouteillon, *J. Appl. Electrochem.* **13** (1983) 277.
[13] S. Traore, Thèse, Grenoble (1984).
[14] R. Monnier, *Helv. Chim.* **37** (1983) 109.
[15] F. R. Clayton, G. Mamantov and D. L. Manning, *J. Electrochem. Soc.* **120** (1973) 1193.
[16] M. E. Sibert and M. A. Steinberg, *ibid.* **102** (1955) 641.
[17] B. J. Fortin, J. G. Wurm, L. Gravel and R. J. A. Potvin, *ibid.* **106** (1959) 428.
[18] A. R. Stetson, *Mat. Des. Eng.* **57** (1963) 81.
[19] K. Matiasowsky, Z. Lubyova and V. Danek, *Electrodep. Surf. Treat.* **1** (1972) 43.
[20] Texas Instruments Inc., Fr. Demande 2 075 857 (1971).
[21] G. A. Kline, European Patent Application 79055 (1983).
[22] J. de Lepinay and P. Pallere, *Electrochim. Acta* **29** (1984) 1243.
[23] R. M. Hansen, 'Constitution of Binary Alloys', McGraw Hill, New York (1958).
[24] S. W. Feldberg, *Electroanal. Chem.* **3** (1969) 199.
[25] A. N. Baraboshkin, Z. S. Martem'yanova, S. V. Plaskin and N. O. Esina, Ext. Abstr. I.S.E. 28th Meeting, Varna (1977).
[26] G. Revel and M. Fedoroff, *Nucl. Instr. Methods* **143** (1977) 277.
[27] P. Paillere, Thèse, Grenoble (1982).
[28] K. B. Oldham, *Anal. Chem.* **44** (1972) 196.
[29] J. C. Imbeaux and J. M. Saveant, *J. Electroanal. Chem.* **44** (1973) 169.